HySAR: Hybrid Material Rendering by an Optical See-Through Head-Mounted Display with Spatial Augmented Reality Projection

Takumi Hamasaki, Yuta Itoh, Yuichi Hiroi, Daisuke Iwai, and Maki Sugimoto

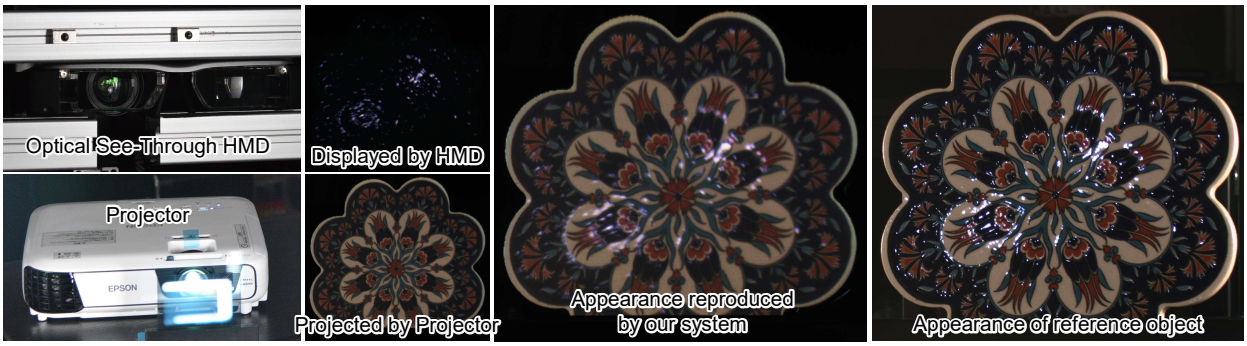

Figure 1. (a) A static projector displays the viewpoint-independent component of the material, and the head-mounted display (HMD) adds the viewpoint-dependent component of the material. (b) Hybrid spatial augmented reality (HySAR) reproduces a reference object with the viewpoint-dependent component and the viewpoint-independent component over multiple viewers. (c) The reference object has a viewpoint-independent component and a viewpoint-dependent component.

Abstract— Spatial augmented reality (SAR) pursues realism in rendering materials and objects. To advance this goal, we propose a hybrid SAR (HySAR) that combines a projector with optical see-through head-mounted displays (OST-HMD). In an ordinary SAR scenario with co-located viewers, the viewers perceive the same virtual material on physical surfaces. In general, the material consists of two components: a view-independent (VI) component such as diffuse reflection, and a view-dependent (VD) component such as specular reflection. The VI component is static over viewpoints, whereas the VD should change for each viewpoint even if a projector can simulate only one viewpoint at one time. In HySAR, a projector only renders the static VI components. In addition, the OST-HMD renders the dynamic VD components according to the viewer's current viewpoint. Unlike conventional SAR, the HySAR concept theoretically allows an unlimited number of co-located viewers to see the correct material over different viewpoints. Furthermore, the combination enhances the total dynamic range, the maximum intensity, and the resolution of perceived materials. With proof-of-concept systems, we demonstrate HySAR both qualitatively and quantitatively with real objects. First, we demonstrate HySAR by rendering synthetic material properties on a real object from different viewpoints. Our quantitative evaluation shows that our system increases the dynamic range by 2.24 times and the maximum intensity by 2.12 times compared to an ordinary SAR system. Second, we replicate the material properties of a real object by SAR and HySAR, and show that HySAR outperforms SAR in rendering VD specular components.

Index Terms—Optical see-through displays, hybrid material rendering, spatial augmented reality

1 Introduction

Spatial augmented reality (SAR) explores how to augment the appearance of real materials [1–3]. In this work, we aim to improve the abilities of SAR by combining it with optical see-through head-mounted displays (OST-HMDs) as a complementary, viewpoint-dependent rendering layer. SAR with projectors is a powerful tool to provide shared augmented-reality (AR) experiences to co-located users. Furthermore, SAR with cameras can reproduce realistic material on physical surfaces. While these two aspects make SAR applications attractive, maintaining both aspects simultaneously is still a challenging task for projector–camera systems.

The problem—or the benefit—of the projector is that its projected image is viewpoint independent (VI). For instance, if a projector casts a metallic material texture on a white diffuse surface by simulating specular properties under a virtual light source [4], the resulting appearance is geometrically valid for only a single viewer (Fig. 2), because the specular component should change based on the virtual viewpoint. An ideal projection mapping must render images tuned to the position of each viewer to resolve the view-point issue. Strictly speaking, even a single viewer cannot see accurate specular reflection without stereo rendering for both eyes. Some SAR systems project different images for each viewer or set of eyes by spatially or temporally multiplexing the projected images [5–7] (Section 2.1). These approaches, however, can not easily increase the number of viewers without compromising the spatial or temporal resolution of the SAR content.

OST-HMDs have features that are complementary to projectors. Because a user wears his/her own OST-HMD, OST-HMDs can display different images to co-located individual users. In other words, we may use OST-HMDs to display viewpoint-dependent (VD) components such as the specular texture of a virtual object. Note that rendering the VD contents requires head tracking, which is becoming readily available in modern HMDs via built-in trackers, such as Microsoft HoloLens.

These capabilities of projectors and OST-HMDs gave us the idea to split the rendering of SAR material in two parts: VI components for projectors and VD components for OST-HMDs. In the common

- *T. Hamasaki, Y. Hiroi, and M. Sugimoto are with Keio University. E-mail: hamasaki, y.hiroi, sugimoto@imlab.ics.keio.ac.jp.*
- *Y. Itoh is with Tokyo Institue of Technology. E-mail: itoh@c.titech.ac.jp.*
- *D. Iwai is with Osaka University. E-mail: daisuke.iwai@sys.es.osaka-u.ac.jp.*

Manuscript received xx xxx. 201x; accepted xx xxx. 201x. Date of Publication xx xxx. 201x; date of current version xx xxx. 201x. For information on obtaining reprints of this article, please send e-mail to: reprints@ieee.org. Digital Object Identifier: xx.xxxx/TVCG.201x.xxxxxxx

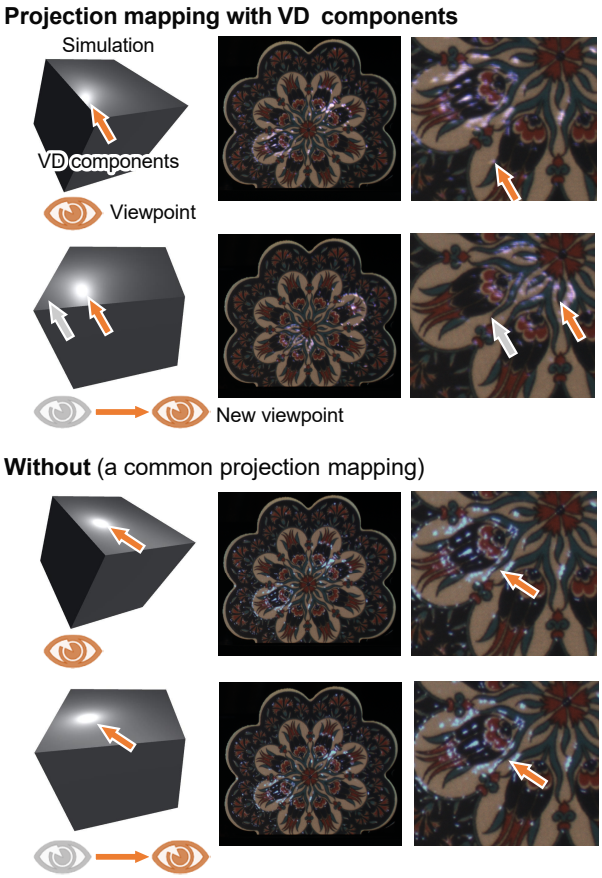

Figure 2. Illustration of material with and without VD components. (Top) Projection mapping with VD components. The specular component changes its appearance as the viewpoint changes. (Bottom) An ordinary SAR setup that projects a texture on the object regardless of the movement of the viewer. VD components stay in the same position because it is a static texture.

material model, known as the dichroic reflection model [8], rendered images in SAR may be separated into the VI component, such as diffuse reflections, and the VD component, including specular reflections. Ordinary SAR is by nature suitable for rendering VI components given diffused surfaces for projection. By definition, the VI components are static over viewpoints and thus do not require knowing the viewer's position for rendering. On the other hand, the VD components dynamically change according to the current viewpoint of a user and must be updated on-line when the viewer moves to a new viewpoint, which is suitable for the capability of OST-HMDs.

This work thus proposes HySAR, a hybrid SAR system that combines an OST-HMD with a projector, with the aim to improve material rendering over that of ordinary SAR systems (Fig. 3). The OST-HMD behaves as an extra rendering layer of SAR to display VD components from a given viewpoint. In addition, we can scale the effective number of viewers without compromising the SAR quality by assigning OST-HMDs for each viewers.

Readers might ask why not just display *all materials* on each OST-HMD or on video see-through HMDs without using SAR. There are several benefits to HySAR over doing this. A practical reason is the visualization quality. OST-HMDs provide brighter images than projectors because projected spatial images are distributed in space and their light is absorbed by surfaces. Consequently, as we demonstrate later, specular reflections can be displayed with much more brightness in HySAR, which leads to more realistic material rendering than using only SAR. Moreover, OST-HMDs could easily achieve a pixel resolution in the viewing angle that exceeds our visual acuity. The displays can thus display much finer images than projectors.

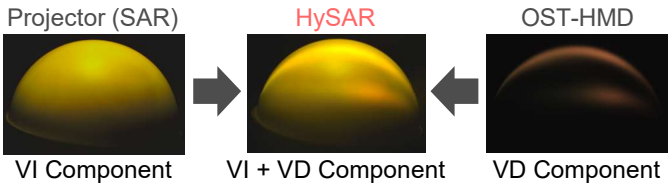

Figure 3. The main concept of HySAR. A VI component are projected by a projector and VD components are displayed by OST-HMDs. HySAR reproduces both components over multiple views, achieving a high dynamic range.

Another reason is that HySAR is theoretically more efficient in terms of sharing material texture data. In practice, VI information such as diffuse components is the main element of material data, whereas VD information such as specular components tend to be local with compact data size when compressed even though the VD components are important for realistic material rendering. If we render all textures for each OST-HMD, the same VI components will be duplicated at the displays; in contrast, using a projector allows the information to be shared. Our HySAR—using OST-HMDs for the VD components and projectors for the VI components—could reduce the entire bandwidth of the whole system and/or reduce the computational power of each OST-HMDs. One may use video see-through HMDs for VD rendering instead of OST-HMDs. This, however, simply deteriorates the view of the real world with projection mapping.

Throughout the paper, using proof-of-concept systems, we first demonstrate HySAR with synthetic material rendering on a real 3D hemispheric object with four different rendering models. In addition to this qualitative evaluation, we also measure how HySAR expands the dynamic range of the rendering and calculate the viewing resolution of the system. The results show that HySAR increases the dynamic range of a conventional SAR system by almost two times and the system can render specular components on the OST-HMD with three times greater viewing angle resolution than the SAR rendering at a given viewpoint. We further reproduce the material of a real reference object by HySAR, SAR, and an OST-HMD. The result shows that HySAR outperforms SAR in rendering VD specular components.

This work focuses on proving the hybrid rendering concept, and the current realization still holds some issues for use in actual SAR applications: our system does not consider color calibration between the OST-HMD and the projector. Our system also does not focus on how to achieve perfectly matched hybrid rendering while the viewer is moving.

Our main contributions include:

- a HySAR concept that combines an OST-HMD with a SAR system for multi-viewpoint material rendering,
- demonstrating the performance of HySAR over conventional SAR (spatial resolution: $\times 2.7$, max. intensity: $\times 2.1$, dynamic range: $\times 2.2$),
- demonstrating the reproduction of a real object's material using HySAR, and
- limitations and guidelines to further improve the quality of the proposed HySAR rendering.

2 Related Work

2.1 Spatial Augmented Reality

Extensive work has been done on changing the appearance of physical objects via SAR. ShaderLamps [2] first demonstrated an attractive result by using projection onto white surfaces shaped arbitrary. In our context, this system simulates only the VI material component on static surfaces.

Several papers have utilized SAR to achieve more realistic material rendering on physical surfaces. The main approach uses multi projector-camera installations to achieve higher resolution [9] and dynamic range [10]. Amano et al. developed a projector-camera system

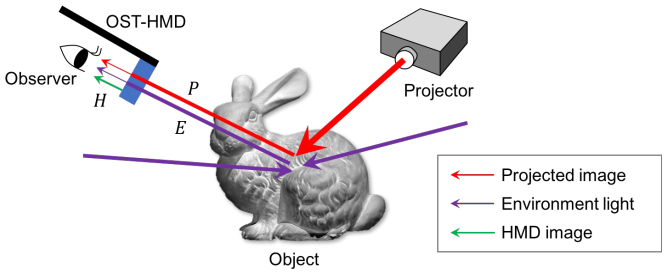

Figure 4. The optical model for HySAR described in Section 3.2. The observed intensity I_{hybrid} is the sum of projected image αP, environment light αE, and OST-HMD image H, where α, $(0 \leq \alpha \leq 1)$ represents the transparency of the HMD.

that manipulates successive material appearance such as color, translucency and glossiness via dynamic projector-camera feedback [11]. Bermano et al. proposed a multi projector-camera system to enhance dynamic expression of a silicone-skin-based head animatronic [12]. Bimber et al. developed a projector-camera system that enhanced the dynamic range of photos by projecting same images as the photos [13]. To support high quality rendering for dynamic contents on complex geometric shapes, Siegl et al. proposed a real-time pixel luminance optimization technique [14]. These studies have achieved attractive texture appearances on physical surfaces. The resulting appearances, however, are valid for only a single viewpoint, and thus they cannot handle multiple viewers. Unlike these single-viewpoint systems, our system renders the VD components dynamically from the current viewpoint of the wearer of an HMD and does not interfere other users' views.

Some SAR systems render different images for each viewer or each eyes of a viewer by rendering multiple images in spatially or temporally multiplexed manners. In an early spatial-multiplexing approach, the Virtual Showcase of Bimber et al.'s displays images on four half-mirror screens with a beam splitter [6]. IllusionHole [15] realizes spatially multiplexed images on a single display with a display mask to provide multiple viewers with views with the correct perspective. Recently, Benko et al. proposed MirageTable [16], which demonstrated VD projections to a single viewer on a dynamically changing real-world scene, and they extended the system in a face-to-face scenario in which two viewers are looking toward each other to cast multiple perspective views [7]. Temporal-multiplexing approaches are commonly combined with active shutter glasses. The glasses are synchronized with projectors to temporally divide the projection into view-individual stereoscopic image pairs from the viewpoint of each wearer [5]. Recently, Koutaki proposed a temporal-multiplexing display to represent multi-view images more accurately by developing a continuous transmittance active shutter system [17].

With the above SAR methodologies, however, the maximum number of viewers is a trade-off with losing spatial or temporal resolution of the SAR contents. A unique approach was presented by Amano et al. [18]. The system realizes VD rendering for multiple viewers simultaneously by applying a retroreflective coating on a real object and projects VD images from multiple projectors situated at different angles. However, the number of viewpoints is restricted by the number of projectors, and the projectors significantly the occlude user's view. Unlike these conventional systems, HySAR theoretically allows an unlimited number of co-located viewers with VD rendering.

2.2 Combining Projectors and OST-HMDs

Some studies combine projectors and OST-HMDs to enhance the appearance of virtual contents. Bimber et al. developed a projector-based lighting control method [19] for Virtual Showcase. In their system, projectors dim the background and create a global illumination around the area where the AR content is displayed in the OST display (a stationary half-silvered mirror AR display). Another system by Maimone et al. used a projector to compensate for the transparency of an OST-HMD by projecting light around the virtual objects seen in the grasses [20]. These works use the projector as an additional smart light source, and do not consider the projector as a viewpoint-independent layer for composed material rendering of objects.

Zhow et al. combined an OST-HMD with a projector for industrial welding applications [21]. In their system, each OST-HMD displays personal 2D information and the projector displays annotation in public by highlighting objects. The OST-HMD only displays texts and images near the position highlighted by the projector. This approach also does not consider the use of an OST-HMD for material rendering.

Our work is conceptually similar to FoveAR [22], which also combines an OST-HMD with projection-based SAR and displays VD components on the OST-HMD. Their system, however, focuses on extending the field of view (FoV) and does not consider improving the quality of material rendering. Unlike their method, which mostly focuses on enriching spatial rendering, our work focuses on a richer material rendering via hybrid VD and VI rendering. In other words, our key idea treats the combination of an OST-HMD and a projector as a hybrid rendering engine equipped with parallel rendering paths for improved material rendering of a single object.

2.3 Changing Physical Material in Real Time

Some interesting studies actually control the material properties of physical surfaces in real time via specialized displays [23]. Hullin et al. presented a dynamic bidirection reflectance distribution function (BRDF) display by the ruffling liquid surface [24]. Ochiai et al. presented a display that dynamically changes brightness and view angle by using a colloidal membrane vibrated by ultrasonic waves [25]. ZoeMatrope [26] can reproduce detailed, spatially-varying materials with composition techniques used in a classical zoetrope. In these systems, VD components can be seen by multiple viewers dynamically without interruption while the viewers are moving around the display. However, these systems cannot easily extend to other objects because of the specialization of the physical displays. Instead, we select the SAR approach as it is easily installed and can be scaled for existing objects.

3 Method

3.1 Separating Material into VI and VD Components

To achieve the hybrid rendering, it is necessary to decompose the material into the VI component and the VD component. We simplify the calculation of material appearance to represent the linear sum of the VI component and the VD component.

In the physically-based rendering (PBR) model, which is commonly used in photo-realistic CG, the material can be decomposed into a VI component and a VD component. The radiance of the reflected light on the object surface is calculated by the rendering equation presented in (1). The outgoing light radiance L_o at a surface point p can be calculated as:

$$L_o(p,v) = L_e(p,v) + \int_{\Omega} f_r(p,l,v) L_i(p,l)(n \cdot l) Vis(p,l) dl \qquad (1)$$

where L_i represents the incident light vector from a point light source l, L_e represents self-emission radiance from p in the direction of a viewer v, n represents the normal vector at p, and Vis represents a visibility function of whether light from l to p is visible. The symbol $\int_{\Omega}$ indicates an integral over a hemisphere of all directions, where f_r represents a spatially varying BRDF, which defines how light is reflected at an opaque surface.

Because the integral over a hemisphere in (1) is hard to solve in real time, we first approximate the light sources to the sum of N light sources that are located at the direction $\{l_1, \ldots, l_N\}$. Furthermore, we deal with only the primary reflection on the surface to decompose L_o into the linear sum of the VI component and the VD component. The di-chromatic reflection model, which can be applied to the primary reflection, assumes that f_r is the sum of the diffuse BRDF $f_d(p,l)$ for the VI component and the specular BRDF $f_s(p,l,v)$ for the VD

Table 1. Qualitative comparison of the three AR approaches (HySAR, SAR only, and OST-HMD only). (*) The full effect of HySAR is only visible in a narrow FOV, but VI components in wider FOV.

	HySAR	SAR	OST-HMD
FOV	**Wide***	**Wide**	Narrow
Spatial resolution	**High**	Low	**High**
Viewpoint-dependent rendering	**Suitable**	Not suitable	**Suitable**
Maximum intensity	**High**	Low	**High**
Dynamic range	**High**	**High**	Low
Color space	**Wide**	Narrow	Narrow

component. Thus, (1) can be rewritten as follows:

$$\begin{aligned} L_o(p,v) &= L_e(p,v)+\textstyle\sum_{i=1}^{N} f_r(p,l_i,v)L_i(p,l_i)(n\cdot l_i)Vis(p,l_i) \\ &= L_e(p,v) \\ &\quad +\textstyle\sum_{i=1}^{N}\{f_d(p,l_i)+f_s(p,l_i,v)\}L_i(p,l_i)(n\cdot l_i)Vis(p,l_i) \\ &= L_e(p,v)+\textstyle\sum_{i=1}^{N}\{L_d(p,l_i)+L_s(p,l_i,v)\} \end{aligned} \quad (2)$$

where $L_d(p,l_i), L_s(p,l_i,v)$ indicate the outgoing diffuse and specular radiance, respectively.

From the result of (2), it is found that a projector should display $L_d(p,l_i)$ as the VI component and the OST-HMD should display $L_s(p,l_i,v)$ and $L_e(p,v)$ as the VD component in our concept of hybrid rendering. If multiple M viewers are dynamically changing their view directions $\{v_1,\ldots,v_M\}$ and each viewer has an OST-HMD, then the display can represent the specular radiance $L_s(p,l_i,v_j)$ for each view direction in real time. Consequently, the viewpoint-dependent radiance L_s displayed by the OST-HMD is added to the viewpoint-independent radiance L_d, and thus the system can simulate wider material expression for multiple viewers.

3.2 Qualitative Performance Comparison

Our hybrid rendering scheme provides better visual AR experiences than conventional projection only and OST-HMD only systems. First, we compare these three approaches in terms of displayable maximum intensity, dynamic range, and color space. We then summarize the comparison with issues already discussed in the previous sections, such as FOV and viewpoint-dependent rendering.

The optical model for the HySAR approach is shown in Fig. 4. The observed intensity I_{hybrid} in this system is the sum of projected image αP, environment light αE, and OST-HMD image H, where $\alpha\,(0\le\alpha\le 1)$ represents the transparency of the HMD. Thus,

$$I_{\text{hybrid}} = H+\alpha(P+E). \quad (3)$$

In the same manner, the observed intensity of SAR (i.e., projection only) I_{SAR} and OST-HMD I_{OST} can be formulated as

$$I_{\text{SAR}} = P+E, I_{\text{OST}} = H+\alpha E. \quad (4)$$

In this section, we assume ordinary environment light conditions for each AR approach. In particular, we assume that the HySAR and SAR systems are used in dark environments (i.e., $E=0$) while the OST-HMD-only system is used under environment light. Suppose that the minimum and maximum intensities displayed by the projector are denoted as P^M and P^m, and intensities displayed by the HMD are H^M and H^m , respectively, the observed maximum intensities I^M and dynamic ranges D are

$$I^M_{\text{hybrid}} = H^M+\alpha P^M, I^M_{\text{SAR}} = P^M, I^M_{\text{HMD}} = H^M+\alpha E, \quad (5)$$

$$D_{\text{hybrid}} = \frac{H^M+\alpha P^M}{H^m+\alpha P^m}, D_{\text{SAR}} = \frac{P^M}{P^m}, D_{\text{HMD}} = \frac{H^M+\alpha E}{H^m+\alpha E}. \quad (6)$$

In a room environment, we can assume $H^M > P^M, E \gg H^m \backsimeq P^m$ without loss of generality. Consequently, the maximum intensities of the HySAR and HMD system are similar, while they are higher than that of SAR. However, the dynamic ranges of the HySAR and SAR system are similar, while they are higher than that of HMD. In addition, the HySAR system can potentially achieve a wider color gamut than SAR and OST-HMD-only systems. In general, spectral properties of the primary colors (i.e., RGB) are different between display devices. Therefore, HySAR would have six primary colors, which can provide more natural color reproduction than ordinary only three primary color displays [27].

The summary of the comparison of the qualitative performance is shown in Table 1, which compares not only the displayable maximum intensity, dynamic range, and color space but also the FOV, spatial resolution, and viewpoint-dependent rendering. From this table, we can confirm that the proposed HySAR system has great advantages over the other conventional approaches. We focus here on the viewpoint-dependent rendering, spatial resolution, maximum intensity, and dynamic range, while the other two elements (e.g., FOV and color space) are the topics of future works.

In the following, we further conduct two experiments to evaluate HySAR: rendering with synthetic data (Section 4) and with data from real material (Section 5).

Figure 5. Overview of the hardware setup of the synthetic rendering experiment (Section 4). (Left) The SAR prop and HoloLens. (Right) The user-perspective camera installed behind the right optical element of the HoloLens.

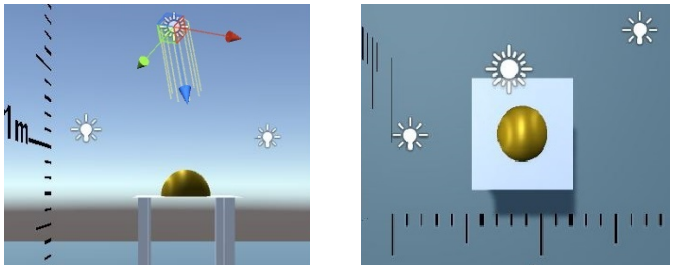

Figure 6. Arrangement of the virtual light sources and the object. (Left) Horizontal view. (Right) Bird's-eye view. We set three virtual white light sources: one directional light and two point lights.

4 Experiment 1: Synthetic Rendering

In this first experiment, we demonstrate the viewpoint-dependent rendering of HySAR using a synthetic dataset.

4.1 Experimental Setup

4.1.1 Hardware Setup

Fig. 5 shows the experimental setup. We prepared a diffuse white hemisphere (30 cm diameter) as an SAR prop to evaluate the composition of the materials (Fig. 5, left). The prop was placed on a desk 69.5cm in height. Ideally, the prop should have a perfect diffuse surface and perfect monochromaticity, like Labsphere Spectralon® diffuse color standards. However, in our experiments, the prop was made of vinyl chloride resin coated with white matte acrylic paint. Therefore, it creates slight specular reflections, has multiple color components, and absorbs some light.

Our system combines a Microsoft HoloLens (30°×17° field of view, 1268×720 pixel for an eye) as an OST-HMD with a ceiling-mounted

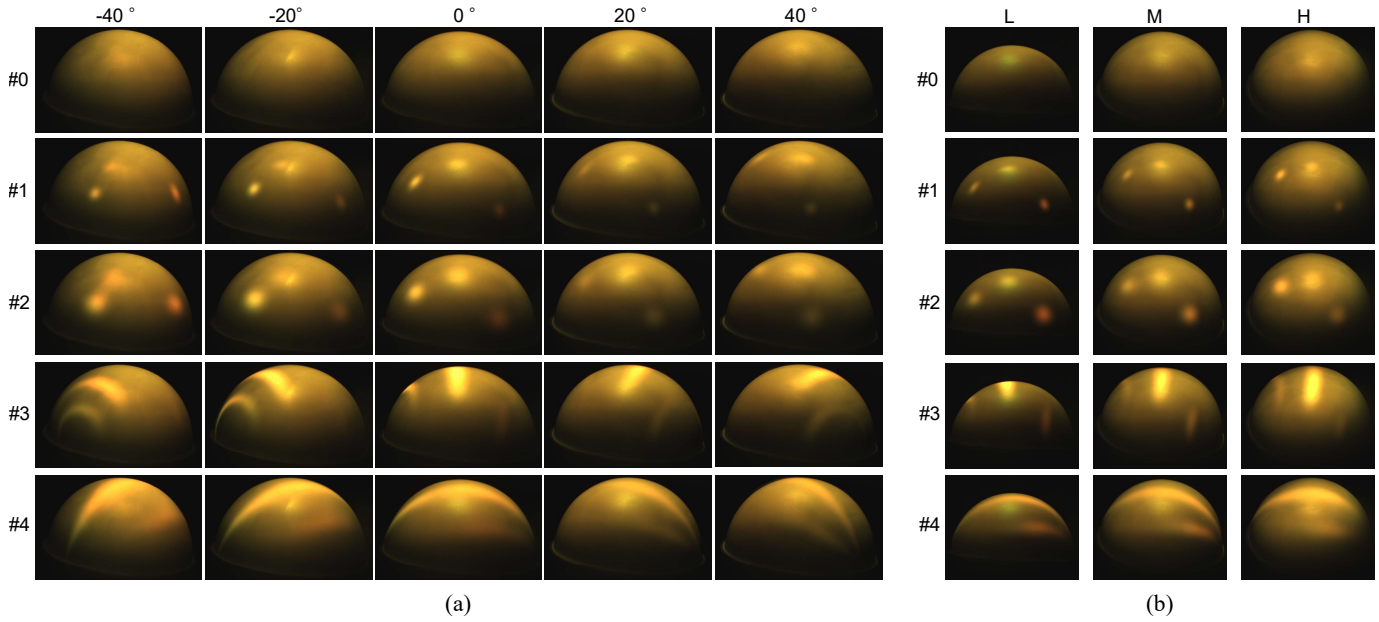

Figure 7. Overview of the results of the simulated rendering. (a) Rendering results with different horizontal view angles (from -40° to 40°). Each column represent a different viewpoint with the horizontal view angle shown. (b) Rendering results with different vertical view angles. Each column represents a different viewpoint with the height shown (H: High, M: Medium, L: Low). For both figures, each row corresponds to #0: Projector (diffuse only), #1: Phong shader, #2: Blinn-Phong shader, #3: Ward shader, and #4: Kajiya-Kay shader.

wide-angle projector (EPSON EB-U32 DLP, 1920×1200 pixel) paired with a Microsoft Kinect v2 depth camera for calibration. The projector and Kinect v2 camera are connected to the same Windows 10 laptop machine (Intel Core i7-6500U CPU 2.50GHz, 8GB RAM), and the Microsoft HoloLens is connected to its integrated Windows 10 machine (Intel Atom CPU 1.04GHz, 2GB RAM). The left panel of Fig. 1 shows the overall hardware setup. To calibrate both the projector and the OST-HMD, Natural Point's OptiTrack Flex 3 system (12 cameras) is hung on the ceiling of the room.

To obtain images from viewpoints through the HoloLens, we installed a user-perspective camera placed behind the right optical element of the display (Fig. 5, right). The camera captures the same scene that would be presented to the user, yet the image is not stereoscopic. For the user-perspective camera, we use Flea 3 FL3-U3-88S2C-C with a resolution of 4096×2160. The subsequent figures are all photographs taken by the camera unless otherwise stated. Both the HoloLens and the user-perspective camera are attached to a tripod. We pasted some stickers on the wall behind the prop to increase the number of feature points in the real scene so that the HoloLens can stably track its position and orientation.

4.1.2 System Calibration

Overlaying virtual content on a real scene requires calibration of both the projection mapping and the OST-HMD rendering.

Calibration for Projection Mapping: In the calibration for the projector, we must estimate the six degrees-of-freedom (6DoF) pose between the motion capture system that tracks the SAR props and the projector through the Kinect v2 cameras. Three calibration steps are required to estimate the pose. First, we calibrated the projector with respect to the Kinect camera by projecting gray code patterns to establish dense correspondences between the Kinect's color camera and the projector. This calibration procedure is described in detail by Jones et al. [28] and is publicly available as the RoomAlive Toolkit. Second, we calibrated the tracking system with respect to the Kinect's color camera. We made a calibration board that has a 10.8×10.8 cm square marker and has three retro-reflective spheres on an acrylic plate. A pose matrix between the AR marker and the center of the spheres was calculated beforehand by hand-eye calibration using the Ubitrack library [29, 30]. Then, we estimated the pose matrix between the tracking system coordinates and the color camera coordinates. Finally, by multiplying poses between the tracking system and the color camera by the pose between the color camera and the projector, we obtained the relative 6DoF pose between the tracking system and the projector.

Calibration for OST-HMD Rendering: In the calibration for the OST-HMD, we have to estimate a pose matrix between the motion capture system and the HoloLens. The appearance of our system is affected by misalignment, as mentioned in Section 6; thus, we manually adjust the pose matrix. First, we aligned the coordinate system displayed in the OST-HMD with the coordinate basis of the motion capture marked on the floor. Then, we finely aligned the virtual contents displayed in the OST-HMD with the SAR prop in the real world. After that, the system renders the image considering the offset between the camera and the glasses by using HoloLens SDK. We manually adjusted the VD component color so that the VD component adapted to the VI component. A parameter optimization for VD components is beyond the scope of this paper, yet we included a related discussion in Sec. 6.

4.1.3 Rendering

We implemented four known specular BRDF models (Phong, Blinn-Phong, Ward, and Kajiya-Kay). The differences of the VD materials between view angles are evaluated with the four models.

For rendering, we set three virtual light sources in the simulation: one directional light and two point lights. The color of all light sources is set to white. The point lights are placed at a height of about 110cm from the floor level. The arrangement of the light sources and the virtual object is shown in detail Fig. 6.

Throughout our experiments, we aimed to reproduce a sheeny yellow metal material such as brass. Normally, specular lights reflected on the surface of a metal are slightly tinged with a particular color. For this reason, we set the colors of the specular lights on the virtual object as yellowish gray for the shading model. It is worth mentioning that without this color adaptation, viewers immediately noticed that the specular rendering on the HMD was fake. Such color matching is not the focus of this paper, but it is an interesting avenue for further exploration in future work. Throughout the experiment, we fixed the material parameters including a specular power, the intensity of each light source, and the luminance of the HoloLens.

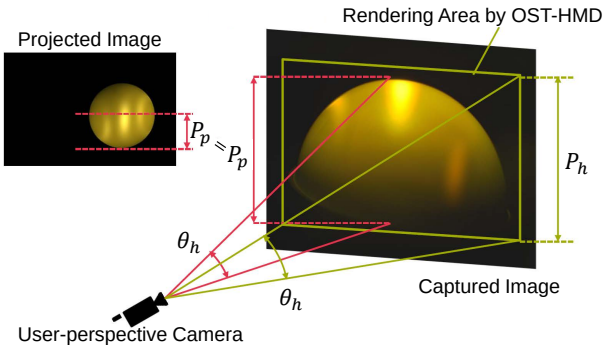

Figure 8. Overview of calculating rendering resolution described in Sec. 4.3. P_p and P_h indicate the numbers of pixels in the rendered region with regard to the projector's and the OST-HMD's resolution. θ_p and θ_h indicate the view angles of each rendered area seen from the user-perspective camera.

We use the Unity 5 game engine for rendering both the projected CG content and the content displayed in the glasses. The Unity engine has its own shader development environment ShaderLab. We implemented the BRDF model in ShaderLab, and separated the model into VI component and VD component in the form of shader scripts.

4.2 Reproduction of Viewpoint-Dependent Materials

To evaluate how well our system reproduces VD material properties during dynamic changes in viewpoint, we compared the rendering results taken from different horizontal view angles (-40°, -20°, 0°, 20°, and 40°) for each BRDF model. The results of the overlaid VD materials are shown in Fig. 7 (a). The virtual VD components displayed by the OST-HMD are obviously shifted, corresponding to the viewpoints. Appropriate parameter optimization of our hybrid rendering system remains for future work as described in Section 6.

Similarly, we compared rendering results with different vertical view angles by changing the height of the tripod (high, medium, low). The results of the overlaid VD materials are shown in Fig. 7 (b). As well as the horizontal view, the virtual VD components are shifted in correspondence with the viewpoints. As a result, our system enhances the virtual material properties, especially when the viewer is moving around the object.

4.3 Comparison of Rendering Resolution

In order to evaluate the difference between the rendering resolutions of the OST-HMD and the projector, we calculated the number of pixels per view angle of the user-perspective camera as shown in Fig. 8. In Fig. 8, P_p indicates the number of pixels in the rendered region with regard to the projector's resolution. Likewise, P_h indicates the number of pixels in the rendered region with regard to the OST-HMD's resolution. The view angles of each rendered area seen from the user-perspective camera are also written as θ_p, θ_h. We then calculated the pixel density for each display device by calculating P_p/θ_p and P_h/θ_h. In our experimental setup, the diffuse component of the hemisphere is rendered as a 480 px diameter circle on the projector image, which implies $P_p = 240$ [px]. The height of the region of the specular component on the OST-HMD is 720 pixel, which implies $P_h = 720$ [px]. The view angles are calculated by the intrinsic parameter of the user-perspective camera, $\theta_p = 10.6$ [deg] and $\theta_h = 11.7$ [deg]. Finally, we calculated the spatial resolution of both devices in the image plane: $P_p/\theta_p = 22.6$ [px/deg] and $P_h/\theta_h = 61.5$ [px/deg] (Table 2).

Considering that the critical gap size of emmetropic (standard) human visual acuity is about 1/60 degree (i.e., the resolution of 20/20 visual acuity is about 60 pixels per degree), the resolution of the VD component on the OST-HMD is comparable to 20/20 visual acuity. In addition to this analysis, our system can theoretically present detailed material properties around the specular component as the OST-HMD has a higher spatial resolution than SAR. If the near-peripheral area is finely expressed, our eyes can obtain more realistic textures on the surfaces around the viewpoint [31]. Based on this "foveated rendering" technique, wherein a narrow FOV display renders in detail and a wide FOV projection renders the entire color of the object, our system is practically suitable for expressing VD materials.

Table 2. Measured resolution, maximum intensity, and dynamic range of HySAR, projector only (i.e., SAR), and OST-HMD only systems with and without environment light described in Sec. 4.4.

			HMD		HySAR /SAR	HySAR /HMD
	HySAR	SAR	E > 0	E = 0		(E > 0)
Resolution [pixel/deg]	**61.5**	22.6	61.5	61.5	×**2.72**	×1.0
Maximum intensity	**4358**	2053	4175	3539	×**2.12**	×1.04
Dynamic range	**137**	61	6	193	×**2.24**	×**21.5**

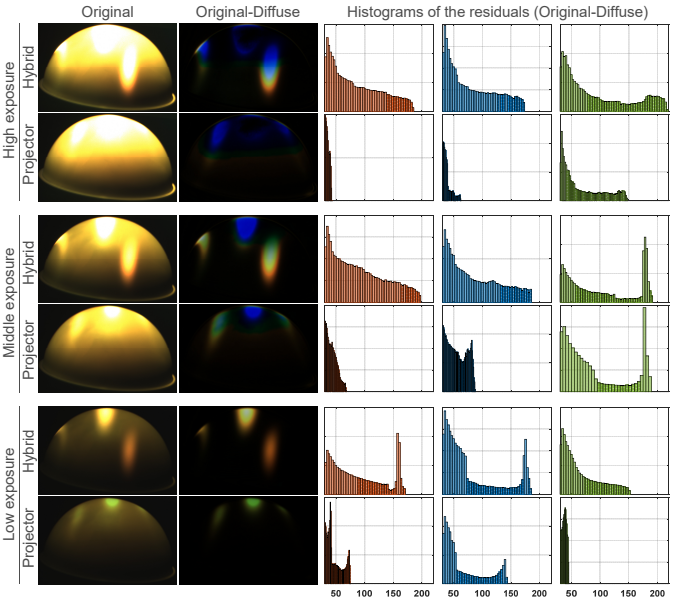

Figure 9. Comparison of the dynamic range of different rendering combinations. First column: The original images captured by the camera. Second column: The specular residuals. Third through Fifth columns: The histograms of the specular residuals in each color channel (red, blue, and green, respectively).

4.4 Comparison of Dynamic Range

We compared the dynamic range of the material rendered by our system and the material rendered only by a projector. First, we captured images by different rendering combinations (projector + HMD hybrid and projector only) with three exposure times (high: 250ms, medium: 125ms, low: 33ms) to evaluate the dynamic range of the specular components. Simultaneously, we captured the diffuse images rendered by the projector. Then we obtained specular residual by subtracting the diffuse images from the original images. Fig. 9 shows the result of the original images, the specular residuals, and the histograms of the specular residual in each color channel (red, blue, and green). In each histogram, we ignored the range of the brightness from 0 to 20 in the figure, as we are interested in the distribution and the maximum brightness of the bright part of the specular residuals.

Compared with the histograms of the residuals from the images rendered only by projector in Fig. 9, the histograms of our system's rendered images clearly show a wider range of brightness. In consequence, our system achieves a higher dynamic range when expressing specular components on the surface for each exposure time. It may be that the lower dynamic range in the specular rendering by the projector is caused by light absorption on the surface, as well as by attenuation of the lights before they reach our eyes. Instead, our system can di-

rectly display the specular component near the viewer's eye, and thus a brighter specular expression can be obtained.

We compare the maximum intensities as well as the dynamic ranges of the HySAR, the projector only (i.e., SAR), and the OST-HMD only systems, respectively. Although OST-HMDs are often used under environment light, we compared the OST-HMD only systems with and without environment light. For the comparison, we measure the parameters discussed in Section 3.2. In particular, they are the maximum and minimum intensities of the projector (P^M and P^m), the maximum and minimum intensities of the OST-HMD (H^M and H^m), the transparency of the OST-HMD (α), and the intensity of the environment light (E). The parameters are measured using our user-perspective camera, which has a linear response, with an appropriate exposure time for which pixel values of the captured image in a region of interest (ROI) are not saturated. We set the ROI as a square region of 100×100 pixels around the center of the hemispherical screen. Then, we average the pixel values in the ROI, and scale it as if it were captured with a specific reference exposure time. In particular, we set the reference exposure time to 1 sec. For example, if the averaged pixel value is measured with an exposure time of 1/60 seconds, then the value is multiplied by 60.

First, we remove the OST-HMD so that the camera directly captures the surface to measure the parameters of the projector. We project a uniform white and black image onto the hemispherical surface, and capture the reflected lights using the camera to measure P^M and P^m, respectively. Second, we turn off the projector and turn on the environment light (i.e., room lights of the experimental room) for measure E (= 637). Third, we replace the OST-HMD in front of the camera to measure αE (α = 0.399). Last, we turn off the environment light and display uniform white and black images on the HMD for measuring H^M and H^m. We set $E = 0$ in the OST-HMD only system without environment light. From the measured parameters, we compute the maximum intensity and the dynamic range of each system using (5) and (6).

Table 2 shows the measured values. We confirmed that HySAR could display both the highest maximum intensity and the highest dynamic range in comparison to the SAR system and the OST-HMD only system with environment light. In particular, its maximum intensity was almost two times higher than that of the projector only system, and its dynamic range was more than 20 times higher than the OST-HMD only system with environment light. The OST-HMD only system without environment light was superior to the HySAR in the dynamic range, because H^m is less than P^m by using the LCD projector and the OST-HMD with OLED, namely Hololens. Using an OLED projector or a laser projector could decrease P^m, and the dynamic range of the HySAR could be more than that of the OST-HMD system without environment light.

5 Experiment 2: Real Material

In this section, we compare HySAR against SAR by reproducing the appearance of real material. The focus of this experiment is to investigate the potential of reproducing VD components by HySAR with real material. This experiment thus does not argue the accuracy of color correction in SAR or of the material appearance estimation, which is another important issue in SAR. Nevertheless, the experiment applies a basic color correction to obtain plausible rendering quality.

5.1 Experimental Setup

5.1.1 Hardware Setup

The top panel in Fig.10 shows the experimental setup. We prepared two mass-produced pottery plates of identical design. We use one plate as a real reference object from which we extract material texture for rendering. We apply a white matte spray on the other plate and use it as a projected diffuse object on which we project the texture (Fig.10 bottom). The reason we prepared a real and a diffuse object of the same shape is to keep their alignment almost identical when we swap them during capturing and rendering steps.

As we need both the VI and the VD component of the reference object, we setup a simple photo-studio layout in a darkroom. At shooting, the camera used in Section 4 captures the real object fixed on a jig at about 1m distance under different lighting conditions. The layout uses two studio light sets and two flashlights. For each light set, we used a Godox SL-100W 2400LUX with a white photo umbrella. The sets cast diffuse light from each side of the object to create the VI component texture. The flashlights, light sources like spotlights, cast beam light from the front of the object to create the VD component texture. The radiance of the flashlights is lower than that of the studio lights, as bright lights increase the radiance of VI components and the radiance of the flashlights is sufficient to create the VD component texture.

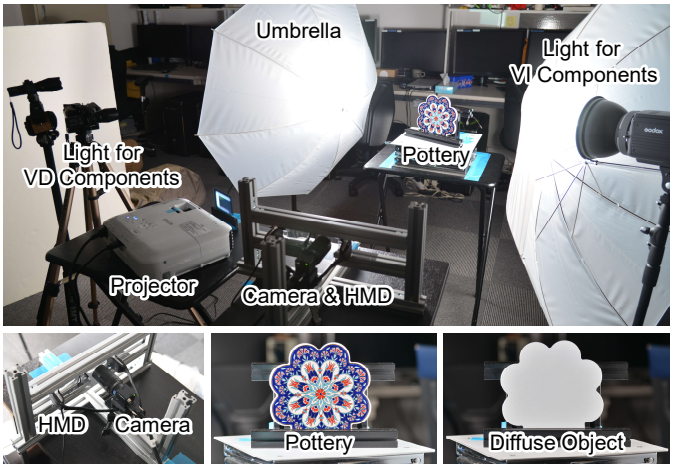

Figure 10. Overview of the hardware setup of the real material experiment (Sec. 5). Studiolights are set for a VI component, and flashlights are set for a VD component. An HMD and a camera are fixed with aluminum frames to capture images from a user-perspective viewpoint. We prepare a piece of pottery as a real reference object to extract textures and another similar piece of pottery with white matte paint to be projected as a diffuse object.

As an OST-HMD, we used an Epson MOVERIO BT-200 (23° field of view, 960×540 pixel for an eye) instead of a Hololens, because a BT-200 is easier to fix with jigs. To output video signal from a PC to the BT-200, we used an interface box, DM484CS (DVI to BT-200 interface). The input image size was set to 1280×720 pixel. We fix the HMD rigidly on an aluminum frame with adhesive glue. To capture images from a user-perspective viewpoint, we installed the camera behind the HMD. The camera focus is set at the real object. A black curtain covered the HMD setup to avoid stray light. Note that, due to the room size, we had to locate the projector in the proximity of the reference or diffuse object. Projected images thus tended to overexpose camera images, which is usually avoided in ordinary SAR setups. We thus placed an ND filter in front of the projector to adjust its dynamic range to that of the camera. As a result, the setup reproduces the intensity of the projector which is not too close to the object.

5.1.2 System Calibration

Spatial Calibration: For correct projection and display by HySAR and SAR, pixel-wise mappings among the camera, the OST-HMD, and the projector are necessary. We compute the mappings by letting the camera capture gray-code patterns on each screen, that is, the OST-HMD screen and the projection surfaces. First, we compute a look-up table (LUT) from the camera image coordinates to the projector image coordinates projected on the diffuse object. From the captured patterns, we first obtain an LUT from the camera to the projector. We apply Gaussian kernel regression on the LUT to compute the inverse mapping. In the same manner, we compute LUTs between the camera image and the HMD image. Note that we had to set the camera aperture smaller during this calibration to avoid off-focus blur due to the mismatch between the HMD screen and the object. This allows the camera to capture the grey-code patterns clearly.

Color Calibration: Colors displayed on a projector and an OST-HMD usually appear different when captured by a camera; therefore,

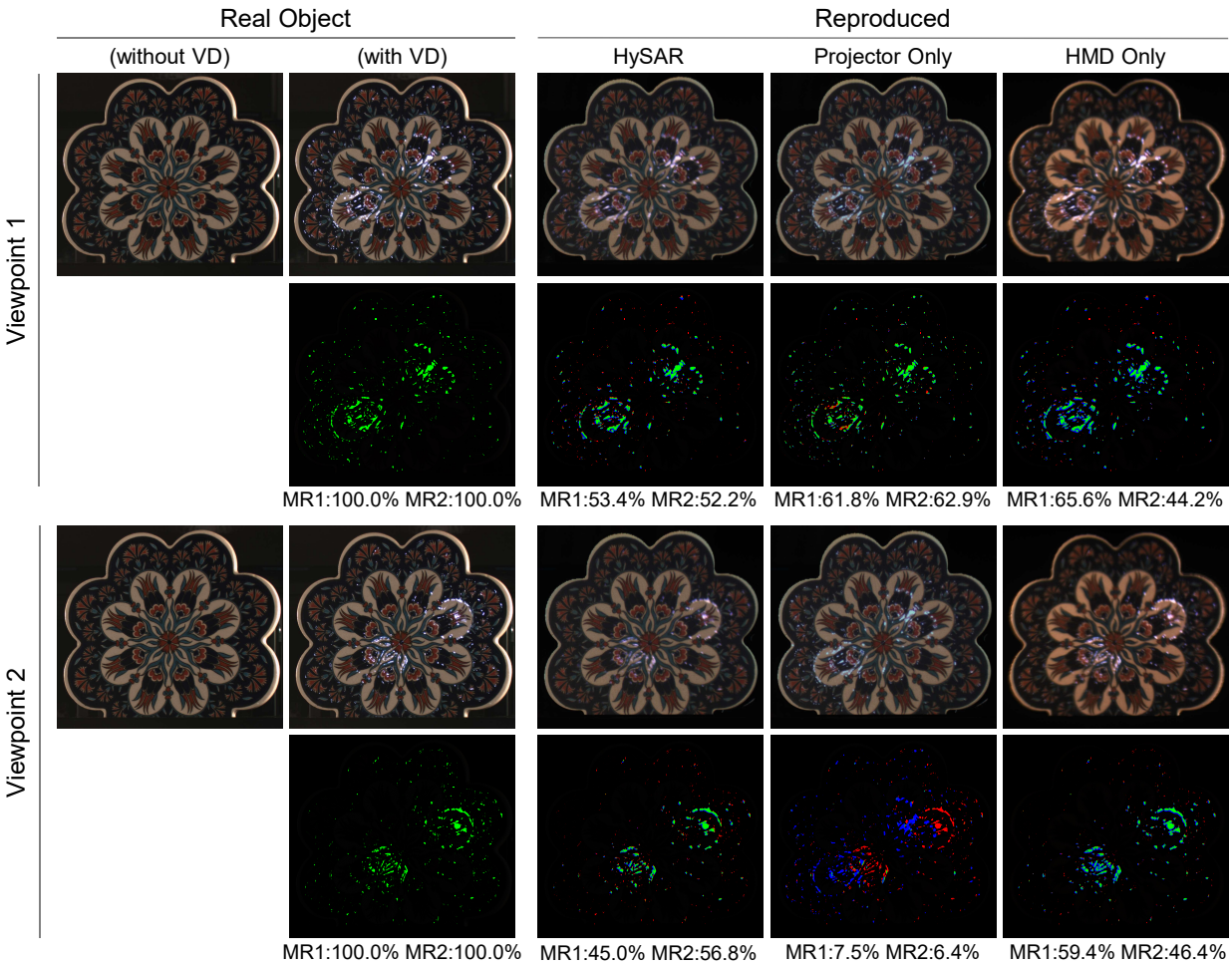

Figure 11. Captured images from two viewpoints in different setups. Lower images in each viewpoint highlight VD areas, with matching area with the true VD area (green), insufficient area with respect to the true area (red), and extra area relative to the true area (blue). MR1 represents how much VD area from a rendered image corresponds to that in the ground-truth image. MR2 represents how much VD area from the ground-truth VD image corresponds to that in the projected image.

we have to correct the color of the projector and the OST-HMD against the camera. We employed two color correction methods: one developed for OST-HMDs [32] and one for projectors [33].

Capturing Material: Once we calibrated the rendering layers, we measure the real object. We placed the real object at the same position as the diffuse object and the camera captured the object while turning on and off the light sources for both the VI component and the VD component. This creates two images of the reference object with different material components: "VI only" and "VI and VD". We obtained a "VD only" image by subtracting the "VI only" image from the "VI and VD" image. Applying the LUTs and color corrections to the captured images generates images to be displayed either on the OST-HMD or the projector to reproduce the VI and/or VD component of the real object. When displaying the generated images, we swap the object to the white, diffuse object and turn off all lighting.

5.2 Comparison with Real Object

We investigate images captured using different setups. In the HySAR setup, we set the VI component on the projector and the VD component on the HMD. In the SAR setup, we only set the "VI and VD" component on the projector, and we left the OST-HMD display black. We also added an HMD-only setup in which the HMD displays the "VI and VD" component. Although beam combiners of the OST-HMD cause distortion for sight and light attenuation slightly, we did not remove the OST-HMD in all setups to conduct the experiment under the same condition. The scope of the experiment is to investigate the quality of VD components reproduced by HySAR, not that of color and brightness.

We repeated the capture from two different viewpoints by moving the OST-HMD workbench. At the second viewpoint, to simulate a scenario wherein SAR does not consider the second viewer, we used the same VD component texture for the source image for the projector to be calibrated. We also used the VI component texture created from the reference object image from the first viewpoint, as the VI component does not change with viewpoints.

Fig.11 shows the results of the experiment. Note that the color of the pottery between Figures 10 and 11 does not match perfectly because we used different cameras. In particular, Figure 11 was captured by an industrial camera, which was used in the experiment because the color calibration of the projector and OST-HMD generally needs to linearize the response and adjust the color balance of the camera for the color calibration [32, 33]. However, Figure 10 was captured by a DSLR camera. In the figure, the images in the first two rows are associated with the first viewpoint, and the images in the other rows are from the second viewpoint. For each viewpoint, the upper images are actual captured images and the lower images are visualizations that highlight the VD areas in different colors by comparing with the reference object image in several ways as follows.

Green areas are the *matching areas* where a VD area in a reproduced image (reproduced HySAR/projector-only/HMD-only in Figure 11) is also in the VD area of the ground-truth VD image (real object with VD in Fig. 11). Red areas are the *insufficient areas* that correspond to the VI areas in a reproduced image even though they are actually detected as VD areas in the ground-truth image. Blue areas are the *extra areas*

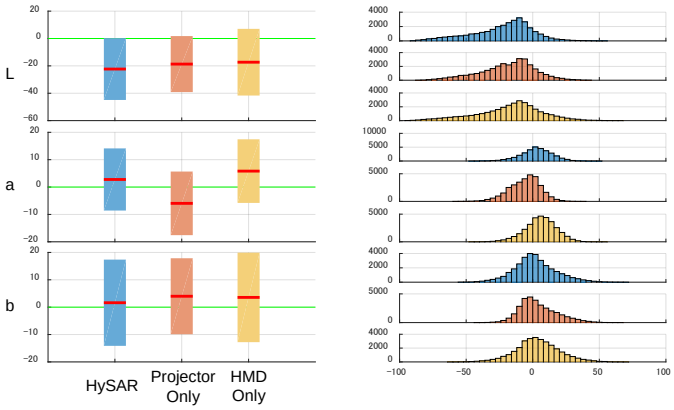

Figure 12. Image quality comparison of HySAR (blue), SAR (red), and the HMD-only setup (yellow). The graphs on the left show the mean and the standard deviation of color difference between images for each method against the reference object image in CIE L*a*b* D65 color space. The graphs on the right show histograms of the differences.

that correspond to the VD areas in a reproduced image even though they are actually VI areas in the ground-truth image. We defined the VD areas as pixels for which all RGB values are 20+ higher than that of the same pixel in the reference images without VD.

By comparing the area size, we define two types of matching ratios (MR): MR1 and MR2. MR1 represents how well the VD area from a reproduced image corresponds to the VD area in the ground-truth image. MR2 represents how much the VD area from the ground-truth VD image is corresponding to the VD area in a projected image. In other words, MR1 is the true positive rate and MR2 is the false positive rate of the VD components. If a reproducing method *mutually and exclusively* reproduces the VD component, both MR1 and MR2 become 100%. As a result, it indicates that HySAR can reproduce VD components whereas SAR cannot.

From the figure, we can see that the VD components of the original images change radically even though the viewpoint change was small. HySAR successfully replicates the VD components when the viewpoint changes (MR1: 53.4%) compared to the SAR setup (MR1: 7.5%). This is expected as the SAR setup did not update the VD component according to the second viewpoint.

Fig.12 shows the pixel-wise color comparisons of VD areas. We compare images of each method against the reference object image. All the images are from the first viewpoint. The VD areas are defined as areas filtered by the threshold mentioned in this paragraph. We first converted the RGB color space to the CIE L*a*b D65 color space and then computed the color difference. The left side of Fig.12 shows the mean and the standard deviation of the color difference, and the right side of Fig.12 shows histograms of the differences. From the figure, the color differences of the mean of the a and the b values in HySAR were closer to 0 than the other methods, and the differences mean of L value did not differ largely from the other methods. Because the standard deviations of HySAR in each Lab value largely overlap with the other methods, it is hard to see clear difference. These lead that decomposing material rendering into two layers: a VD components layer and a VI components layer, do not largely affect quality of the rendering.

From this experiment, we can see that the HySAR method reproduces the color of the reference object at a level least at a similar to that of the other two methods. However, as indicated in Section 4, HySAR still outperforms the other two methods in terms of the resolution, maximum intensity, and dynamic rage.

6 Limitations and Future Work

Color Correction for the Devices and the SAR Prop: We mainly focus on the HySAR system for VD material rendering in this paper. Optimizing the rendering parameters to enrich the material composition still remains as a challenging task. A nonlinear color correction technique [34] can display more accurate colors than the linear techniques we applied in this paper [32, 33]. Compensation regarding the real light sources is necessary to provide more immersive materials. Looking at the result of the diffuse-only rendering in Fig. 7, we can see specular components made by light sources in real scenes (mainly caused by the projector light), as the SAR prop does not have a perfectly diffuse surface nor is perfectly monochromatic, as mentioned in Section 4.1. A radiometric compensation proposed by Wetzstein et al. [35] could adjust projector images so that the SAR prop appears as perfectly diffuse surface. We are interested in an approximation to compensate the roughness of the available bases, similar to the function proposed by Miyasita et al. for their ZoeMatrope system [26]. Similarly, the imperfections in the OST-HMD optics caused by channel-wise image shift and blur degrade the specular expression. For instance, some of the specular texture in Fig. 7 is tinged with red. Itoh et al. [36] have recently demonstrated a promising approach to compensating image shift and blur in OST-HMDs.

Parameter Optimization for Focusing and Shading: Although the spatial position of the VD component rendered by projection is at the correct position on the real surface, in the case of hybrid rendering, the VD component is displayed on the focal plane of the OST-HMD, which is far from the correct surface. As a result, the specular component rendered by our system is partially more vivid and sharper than in the virtual scene. Fortunately our system can display binocular parallax images on the OST-HMD, and thus the specular component can be defocused according to the depth of the contents to obtain spatial consistency. Also, in order to reproduce the specular reflection in the virtual scene onto the real object, the parameters in each shader, such as specular power and color, remain to be optimized in future work.

Alignment of the Components between Devices: The alignment of the components between the images displayed by the OST-HMD and the projector in the 2D image plane is important, especially as the specular image covers the rim of the object (Fig. 7). In the current setup, because the position of the HoloLens is tracked by its color and depth cameras, the contents are easily misaligned when using fewer feature points for tracking. One simple solution is attaching some retro-reflective markers to the OST-HMD, yet the space available for the viewer to move will be limited. Furthermore, the tracking requires low latency since large latency causes the misalignment. Implementing a more stable and lower-latency self-localization algorithm in the OST-HMD will enhance our hybrid material expression in the future.

SAR Rendering against HySAR: To highlight the difference between SAR and HySAR, we summarize their complementary advantages in terms of image rendering. The main strength of SAR against HySAR is its ideal geometrical registration between the VD and VI components. First, SAR needs no additional alignment when overlaying the VD component on the VI component at the appropriate viewpoint because SAR renders both components at the same time. It is also trivial for SAR to render the VI component on the surface depth compared to HySAR, where the OST-HMD displays the images on the plane, and not on the physical surface.

However, HySAR has the following advantages. As we repeatedly mentioned, HySAR allows real-time VD rendering from a theoretically unlimited number of viewers' positions. HySAR could achieve richer material expression with high dynamic range and binocular rendering in the OST-HMD. Furthermore, HySAR can present VD components in high resolution. As VD components could be small, yet complex in appearance, such as specular reflections, this advantage is desirable.

Viewpoint Dependency: Throughout this paper, we considered common diffuse and specular materials for the VD and the VI component respectively. Since the lighting in the real world is significantly more complex, one could consider applying more sophisticated rendering models. For example, under Fresnel reflection [37], the brightness of a reflected light is dependent on both the refraction index of the surface and the angle of the incident light. When the incident angle is relatively low, the reflection intensity appears almost constant independent of the viewing angle. Contrarily, when the angle is large enough,

the Fresnel reflection radically changes the reflection intensity depending on the angle. In the former case, the component could be included in the VI component and in the latter case in the VD component. Note that we should subtract this VI component as an offset from the VD component when we split the Fresnel reflection into the VD and the VI components.

7 Conclusion

We proposed a hybrid spatial augmented reality (HySAR) concept that combines an OST-HMD with SAR. In HySAR a projector renders the viewpoint-independent component as is and OST-HMDs render the viewpoint-dependent components corresponding ideally to an unlimited number of co-located viewers. This splitting of the rendering components could allow richer material rendering and could yield computational efficiency compared to ordinary SAR. The evaluations with real objects presented here show that the system achieves high-dynamic range and high resolution material expression, and demonstrates material rendering with higher fidelity in the specular components. We believe that HySAR shows the potential for extending conventional material expressions in SAR.

8 Acknowledgments

This work was partially supported by JSPS KAKENHI Grant Numbers JP15H05925, JP17H04692 and JP17K19985, and by JST CREST Grant Number JPMJCR14E1, Japan.

References

[1] O. Bimber and R. Raskar, *Spatial augmented reality: merging real and virtual worlds*. CRC press, 2005.

[2] R. Raskar, G. Welch, K.-L. Low, and D. Bandyopadhyay, "Shader lamps: Animating real objects with image-based illumination," in *Rendering Techniques 2001*, pp. 89–102, Springer, 2001.

[3] T. Okazaki, T. Okatani, and K. Deguchi, "A projector-camera system for high-quality synthesis of virtual reflectance on real object surfaces," *Information and Media Technologies*, vol. 5, no. 2, pp. 691–703, 2010.

[4] M. Broecker, B. H. Thomas, and R. T. Smith, "Adapting ray tracing to spatial augmented reality," in *The 13th IEEE ISMAR*, pp. 1–6, IEEE, 2013.

[5] M. Agrawala, A. C. Beers, I. McDowall, B. Fröhlich, M. Bolas, and P. Hanrahan, "The two-user responsive workbench: support for collaboration through individual views of a shared space," in *The 24th ACM SIGGRAPH*, pp. 327–332, ACM Press/Addison-Wesley Publishing Co., 1997.

[6] O. Bimber, B. Fröhlich, D. Schmalstieg, and L. M. Encarnação, "The virtual showcase," in *ACM SIGGRAPH 2006 Courses*, p. 9, ACM, 2006.

[7] H. Benko, A. D. Wilson, and F. Zannier, "Dyadic projected spatial augmented reality," in *The 27th ACM UIST*, pp. 645–655, ACM, 2014.

[8] S. A. Shafer, "Using color to separate reflection components," *Color Research & Application*, vol. 10, no. 4, pp. 210–218, 1985.

[9] D. G. Aliaga, Y. H. Yeung, A. Law, B. Sajadi, and A. Majumder, "Fast high-resolution appearance editing using superimposed projections," *ACM ToG*, vol. 31, no. 2, p. 13, 2012.

[10] A. Majumder and G. Welch, "Computer graphics optique: Optical superposition of projected computer graphics," in *Eurographics Workshop on Rendering*, pp. 209–218, 2001.

[11] T. Amano, "Projection based real-time material appearance manipulation," in *Proceedings of the IEEE Conference on Computer Vision and Pattern Recognition Workshops*, pp. 918–923, 2013.

[12] A. Bermano, P. Brüschweiler, A. Grundhöfer, D. Iwai, B. Bickel, and M. Gross, "Augmenting physical avatars using projector-based illumination," *ACM ToG*, vol. 32, no. 6, p. 189, 2013.

[13] O. Bimber and D. Iwai, "Superimposing dynamic range," *ACM ToG*, vol. 27, pp. 150:1–150:8, Dec. 2008.

[14] C. Siegl, M. Colaianni, L. Thies, J. Thies, M. Zollhöfer, S. Izadi, M. Stamminger, and F. Bauer, "Real-time pixel luminance optimization for dynamic multi-projection mapping," *ACM ToG*, vol. 34, no. 6, p. 237, 2015.

[15] Y. Kitamura, T. Nakayama, T. Nakashima, and S. Yamamoto, "The illusionhole with polarization filters," in *Proceedings of the ACM Symposium on Virtual Reality Software and Technology*, VRST '06, (New York, NY, USA), pp. 244–251, ACM, 2006.

[16] H. Benko, R. Jota, and A. Wilson, "Miragetable: freehand interaction on a projected augmented reality tabletop," in *Proceedings of the SIGCHI conference on human factors in computing systems*, pp. 199–208, ACM, 2012.

[17] G. Koutaki, "Binary continuous image decomposition for multi-view display," *ACM ToG*, vol. 35, no. 4, p. 69, 2016.

[18] T. Amano and K. Minami, "Structural color display on retro-reflective objects," in *International Conference on Artificial Reality and Telexistence and Eurographics Symposium on Virtual Environments*, pp. 37–44, 2015.

[19] O. Bimber, A. Grundhöfer, G. Wetzstein, and S. Knödel, "Consistent illumination within optical see-through augmented environments," in *The 2nd IEEE/ACM ISMAR*, pp. 198–207, IEEE Computer Society, 2003.

[20] A. Maimone, X. Yang, N. Dierk, A. State, M. Dou, and H. Fuchs, "General-purpose telepresence with head-worn optical see-through displays and projector-based lighting," in *2013 IEEE Virtual Reality*, pp. 23–26, IEEE, 2013.

[21] J. Zhou, I. Lee, B. Thomas, R. Menassa, A. Farrant, and A. Sansome, "In-situ support for automotive manufacturing using spatial augmented reality.," *International Journal of Virtual Reality*, vol. 11, no. 1, 2012.

[22] H. Benko, E. Ofek, F. Zheng, and A. D. Wilson, "Fove ar: Combining an optically see-through near-eye display with projector-based spatial augmented reality," in *The 28th ACM UIST*, pp. 129–135, ACM, 2015.

[23] M. B. Hullin, I. Ihrke, W. Heidrich, T. Weyrich, G. Damberg, and M. Fuchs, "Computational Fabrication and Display of Material Appearance," in *Eurographics 2013 - State of the Art Reports* (M. Sbert and L. Szirmay-Kalos, eds.), The Eurographics Association, 2013.

[24] M. B. Hullin, H. P. A. Lensch, R. Raskar, H.-P. Seidel, and I. Ihrke, "Dynamic display of brdfs," *Computer Graphics Forum*, vol. 30, no. 2, pp. 475–483, 2011.

[25] Y. Ochiai, A. Oyama, and K. Toyoshima, "A colloidal display: membrane screen that combines transparency, brdf and 3d volume," in *ACM SIGGRAPH 2012 Emerging Technologies*, p. 2, ACM, 2012.

[26] L. Miyashita, K. Ishihara, Y. Watanabe, and M. Ishikawa, "Zoematrope: a system for physical material design," *ACM ToG*, vol. 35, pp. 66:1–66:11, July 2016.

[27] I. Kauvar, S. J. Yang, L. Shi, I. McDowall, and G. Wetzstein, "Adaptive color display via perceptually-driven factored spectral projection," *ACM ToG*, vol. 34, pp. 165:1–165:10, Oct. 2015.

[28] B. Jones, R. Sodhi, M. Murdock, R. Mehra, H. Benko, A. Wilson, E. Ofek, B. MacIntyre, N. Raghuvanshi, and L. Shapira, "Roomalive: magical experiences enabled by scalable, adaptive projector-camera units," in *The 27th ACM UIST*, pp. 637–644, ACM, 2014.

[29] M. Huber, D. Pustka, P. Keitler, F. Echtler, and G. Klinker, "A system architecture for ubiquitous tracking environments," in *The 6th IEEE/ACM ISMAR*, pp. 1–4, IEEE Computer Society, 2007.

[30] J. Newman, M. Wagner, M. Bauer, A. MacWilliams, T. Pintaric, D. Beyer, D. Pustka, F. Strasser, D. Schmalstieg, and G. Klinker, "Ubiquitous tracking for augmented reality," in *The 3rd IEEE/ACM ISMAR*, pp. 192–201, IEEE, 2004.

[31] H. Hua and S. Liu, "Dual-sensor foveated imaging system," *Applied optics*, vol. 47, no. 3, pp. 317–327, 2008.

[32] Y. Itoh, M. Dzitsiuk, T. Amano, and G. Klinker, "Semi-parametric color reproduction method for optical see-through head-mounted displays," *IEEE TVCG*, vol. 21, no. 11, pp. 1269–1278, 2015.

[33] T. Yoshida, C. Horii, and K. Sato, "A virtual color reconstruction system for real heritage with light projection," in *Proc. International Conference on Virtual Systems and Multimedia*, pp. 161–168, 2003.

[34] A. Grundhöfer and D. Iwai, "Robust, error-tolerant photometric projector compensation," *IEEE Transactions on Image Processing*, vol. 24, no. 12, pp. 5086–5099, 2015.

[35] G. Wetzstein and O. Bimber, "Radiometric compensation through inverse light transport," in *Proceedings of the 15th Pacific Conference on Computer Graphics and Applications*, pp. 391–399, IEEE Computer Society, 2007.

[36] Y. Itoh, T. Amano, D. Iwai, and G. Klinker, "Gaussian light field: Estimation of viewpoint-dependent blur for optical see-through head-mounted displays," *IEEE TVCG*, 2016.

[37] J. F. Blinn, "Models of light reflection for computer synthesized pictures," in *ACM SIGGRAPH Computer Graphics*, vol. 11, pp. 192–198, ACM, 1977.